AIAA 2001–0451

Numerical Study of Turbulent Flow Around a Rotating Cylinder with Backward-Facing Steps

Kyung-Soo Yang and Jong-Yeon Hwang
Department of Mechanical Engineering, Inha University, Inchon, 402-751, Korea

Klaus Bremhorst and Srdjan Nesic
Department of Mechanical Engineering, The University of Queensland, Brisbane, Qld 4074, Australia

39th AIAA Aerospace Sciences Meeting and Exhibit
8–11 January 2001/Reno, NV

Numerical Study of Turbulent Flow Around a Rotating Cylinder with Backward-Facing Steps

Kyung-Soo Yang*and Jong-Yeon Hwang†
Department of Mechanical Engineering, Inha University, Inchon, 402-751, Korea
Klaus Bremhorst‡and Srdjan Nesic§
Department of Mechanical Engineering,
The University of Queensland, Brisbane,
Qld 4074, Australia

Abstract

Erosion-corrosion in a pipe system often occurs at fittings, valves, and weld beads where flow separation and reattachment yield high turbulence intensity. Thus identifying their correlations would be the first step towards resolving the erosion-corrosion problems associated with industrial applications. In an earlier work, we proposed that a rotating cylinder with surface roughness (two backward-facing steps periodically mounted on a circular cylinder) be an economical and tractable tool which can generate extreme flow conditions for erosion-corrosion study. In this work, DNS has been carried out for turbulent flow around the same rotating cylinder as the experimental apparatus used in the previous study. The aim of this paper is to elucidate the flow characteristics associated with this particular configuration. The numerical result shows that a region of intense turbulence intensity and high wall-shear stress fluctuation is formed along the cylinder surface in the recirculating region downstream of the step, where high mass-transfer capacity is also experimentally observed. Since corrosion is mass-transfer controlled, our finding sheds light on the direction of future corrosion research.

Introduction

Corrosion is often found in mechanical and/or chemical processes, especially at fittings, valves, and weld beads in a pipe system, and has to be under control from the safety and economical points of view.[1–3] For example, rust which is formed by oxidization on the inner surface of metal pipe plays an important role as a protective film for the pipe. However, this film gets thinner and thinner due to erosion and dissolution. Erosion is caused by mechanical actions such as turbulence or wall-shear stresses, impingement of bubbles or droplets, and cavitation. On the other hand, dissolution is a chemical mechanism explained by mass transfer of rust into the main flow. When the film is completely removed by the two mechanisms, the raw metal of the pipe is again exposed to the solution. Repeated cycles of the formation and removal of the protective film may result in perforation through the pipe wall; this can be a hazardous situation if the solution is toxic or radioactive.

Turbulence not only plays an important role in erosion, but also indirectly influence the dissolution of a protective film by enhancing the mass transport into the main flow stream via turbulent mixing. In practice, corrosion in aqueous solutions is known to be mass transfer controlled.[1,2] However, mass transfer in complex flow geometries where flow separation and reattachment yield high turbulence intensity, is strongly influenced by the local fluid dynamic conditions such as turbulence. Therefore, corrosion in a pipe system is closely related to turbulence in the flow fields, and identifying their correlations would be the first step towards resolving corrosion problems.

Laboratory investigations into the velocity sensitivity of corrosion can use a number of means of establishing a velocity field for testing. Unfortunately, not all methods lead to well defined fluid dynamic conditions.[4] Fully developed pipe flows, annular flow and impinging jets are amongst the best defined conditions. For most testing, these require expensive testloops and large amounts of test fluid and are difficult to control for more sophisticated tests involving electrochemical studies. A much more practical arrangement is the rotating cylinder electrode which will allow easy testing even at elevated temperatures and pressure by use of autoclaves. Silverman[4] has determined the equivalence of a smooth rotating cylinder

*Associate Professor, AIAA member,
†Graduate Student,
‡Professor,
§Senior Lecturer.

electrode to fully developed pipe flow for identical mass transfer coefficients. This was achieved by use of relevant mass transfer correlations for pipe flow and for rotating cylinder flow. However, since only smooth surfaces are generally used, only low corrosion rates result. In processing plants such as used, for example, in the production of alumina, highly accelerated corrosion rates are found at tube inlets of heat exchangers, valves and behind baffles near the flow reattachment region.

For easy generation of extreme flow conditions, a rotating cylinder with surface-mounted two-dimensional backward-facing steps was proposed and its mass-transfer characteristics were experimentally studied in detail.[5] The objectives of this Direct Numerical Simulation (DNS) are two-fold; firstly to describe the fluid dynamic characteristics of the turbulent flow associated with the rotating cylinder in detail, and secondly to identify any differences between the conventional plane backward-facing step flow[6,7] and the current one.

Formulation

In this study, computations were carried out with respect to a reference frame rotating with a constant angular velocity(Ω). The governing incompressible continuity and momentum equations are

$$\nabla \cdot \mathbf{u} = 0 \tag{1}$$

$$\frac{\partial \mathbf{u}}{\partial t} + (\mathbf{u} \cdot \nabla)\mathbf{u} = -\frac{1}{\rho}\nabla \mathrm{P} + \nu \nabla^2 \mathbf{u} - 2\boldsymbol{\Omega} \times \mathbf{u} \tag{2}$$

where $\mathbf{u}$, ρ, and ν denote velocity, density, and kinematic viscosity, respectively. Turbulence modelling is not included; all scales are resolved using a fine grid. The last term in Eq. (2) represents the Coriolis force. Since the centrifugal force is conservative, it is included in the pressure term, and does not affect the velocity field.[8] Thus, P in Eq. (2) includes not only pressure but also the centrifugal potential. The governing equations were discretized using a finite-volume method in a generalized coordinate system. Spatial discretization is second-order accurate. A hybrid scheme is used for time advancement; nonlinear terms and cross diffusion terms are explicitly advanced by a third-order Runge-Kutta scheme, and the other terms are implicitly advanced by the Crank-Nicolson method. A Fractional Step Method[10] is employed to decouple the continuity and momentum equations. For the details of the numerical algorithm used in the code, see Rosenfeld *et al.*[10] Unless specified otherwise, all the flow variables are normalized by the step height (h) and the circumferential speed of the cylinder surface upstream of the step (U_o) as the length and velocity scales, respectively.

Choice of Numerical Parameters

Simulation was performed for the rotation with Ω=2,000rpm in the air. The shape of the cylinder cross-section was taken exactly the same as that of the central part of the cylinder in the experiment.[5] Since the steps are mounted symmetrically with respect to the axis of rotation, only one half of the domain is considered with the periodic boundary condition in the circumferential direction. The axial (spanwise) direction (z) was assumed as homogeneous. The outer boundary of the computational domain is located approximately 3 diameters ($0.07m$) away from the center of rotation, and the spanwise size (W) of the domain is approximately one diameter ($0.024m$). The step height is $0.002m$. Figure 1 shows the computational grid employed in this study. Figure 1(a) exhibits the whole computational domain at one cross-section in the axial direction, and Fig. 1(b) is a magnified view around the cylinder. The grid is a body-fitted O-grid system which is the most suitable for this complicated geometry, with more resolution near the steps and solid boundaries. The number of grid points was progressively refined using grid-refinement study up to 224 × 128 × 80 in the circumferential, normal, and spanwise directions. Based on the friction velocity(u_τ) at the location $3h$ upstream of the step, the minimum and maximum grid spacing in each direction is Δ^+_{min}=0.0174, Δ^+_{max}=3.18 in the circumferential direction, Δ^+_{min}=0.0086, Δ^+_{max}=0.67 in the normal direction, and Δ^+_z=4.7 in the spanwise direction, respectively. One typical run including statistical evaluation takes about 12,000 time steps which correspond to 10 revolutions of the cylinder, and one time step takes approximately 50 seconds on a CRAY C90 supercomputer.

Initial and Boundary Conditions

With respect to the rotating reference frame, the inner cylinder is stationary while the outer circular boundary is rotating in the clockwise direction. The initial flow field was constructed such that at any location in the flow field, the velocity was given as Ω times the distance between the point and the center of rotation. This is an obvious choice because in the laboratory the cylinder starts rotating in stationary ambient air. In addition, a small-amplitude random noise of which root-mean-squared magnitude was approximately 0.1% of U_o was added only at the beginning of the simulation in order to bypass transitional regime and to establish a self-sustaining turbulence as quickly as possible.

The no-slip boundary condition was applied on the surface of the cylinder and a periodic boundary condition was employed in the homogeneous spanwise direction. The outer boundary condition needs a special attention. One could impose a constant circumferential speed of Ωr_o, where r_o is the outer radius of the

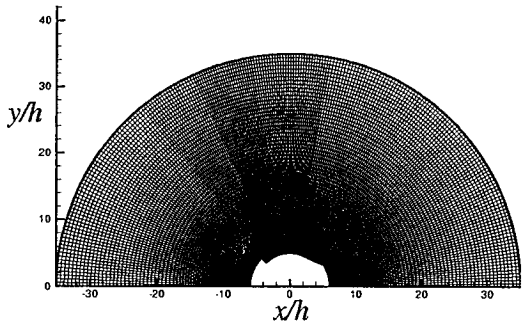

a) Total view.

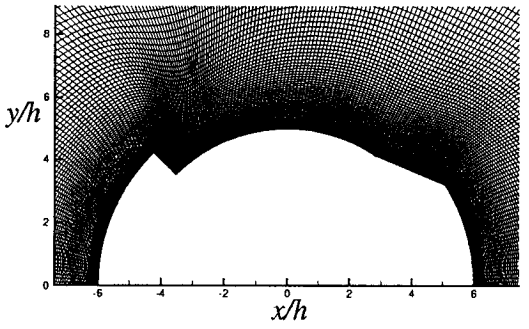

b) Magnified view.

Fig. 1 Cylinder cross-section and grid system employed.

domain, on the outer boundary. This corresponds to the situation that the outer boundary is located far way from the cylinder such that the air at the outer boundary is not disturbed by the motion of the cylinder. From the numerical point of view, this requires a large computational domain with a fine resolution near the outer boundary which is not the region of our interest. This will result in a significant waste in computational resources. To minimize such a waste, a proper boundary condition was devised and employed on the outer boundary. That is,

$$\frac{\partial v_\theta}{\partial n} = \Omega, \quad v_r = 0, \quad \frac{\partial v_z}{\partial n} = 0, \tag{3}$$

where v_θ, v_r, and v_z represent the circumferential, normal, and spanwise velocity components, respectively, and n denotes the direction locally perpendicular to the outer boundary. This boundary condition allows us a reasonably-small computational domain without significantly disturbing the flow field near the cylinder which is the region of our primary interest. Furthermore, since the circumferential velocity gradient is exactly specified at the boundary, rather than computed during the simulation, a fine numerical resolution is not required near the outer boundary, which leads us to an additional saving in CPU time.

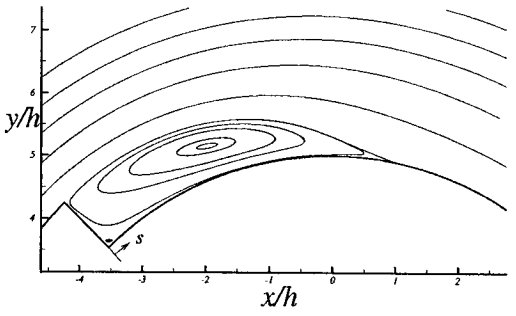

Fig. 2 Mean flow field near the step; streamlines.

Results and Discussion

Averaged velocity fields

After the flow reached a statistically steady state, collecting of instantaneous flow fields was initiated for statistical evaluation. Averaging of the flow variables was carried out in the homogeneous axial direction and also in time. More than 160 instantaneous flow fields were collected over 7 revolutions of the cylinder.

The averaged streamlines in the vicinity of the step are shown in Figure 2. The main recirculating region and a secondary one near the corner can be clearly identified. Figure 2 confirms that this flow geometry will create a qualitatively similar flow pattern, as observed near a sudden pipe expansion or a plane backward-facing step, including flow separation and reattachment. The mean reattachment point is located at s/h=4.9 where s is the coordinate axis along the cylinder surface as indicated in Fig. 2.

The distributions of the averaged circumferential and axial wall-shear stresses ($\overline{\tau}_{w_s}$ and $\overline{\tau}_{w_z}$, respectively, where the overbar means averaging both in z and in time) are shown in Fig. 3. The wall-shear stresses are normalized by an upstream $\overline{\tau}_{w_s}$ at s=-4 ($\overline{\tau}_{w_s,in}$). The coarse-grid (64 × 64 × 32) result considerably deviates from those of the other fine-grid (112 × 96 × 64, 224 × 128 × 80) computations in terms of the shape of $\overline{\tau}_{w_s}$ distribution and the location of the reattachment point. Since the wall-shear stress is very sensitive to numerical resolution, Fig. 3 indicates that the finest grid (224 × 128 × 80) should be suitable for our main simulation. The maximum $|\overline{\tau}_{w_s}|$ in the main recirculating region ($|\overline{\tau}_{w_s}|_{max}$), and the reattachment point where $\overline{\tau}_{w_s}$=0 are identified at s/h=2.9 and s/h=4.9, respectively. The sharp peak at s/h=9.2 is corresponding to the sharp corner in Fig. 1(b) near x/h=5.1 far downstream of the step. This protruding part is necessary to re-establish the flow for the next step located exactly opposite to the step shown in Fig. 1(b). Recall that the cylinder is symmetric with respect to the axis of rotation. Around s/h=−4 which corresponds to three step heights upstream of the sharp edge of the step, $\overline{\tau}_{w_s}$ is nearly constant; u_τ at this location was employed for the normalization

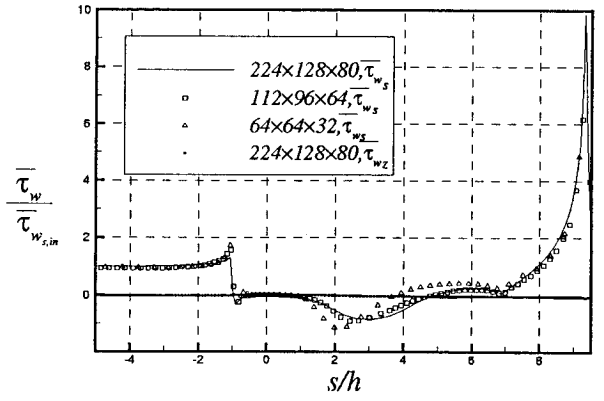

Fig. 3 Distribution of the mean wall-shear stress; $\overline{\tau}_{w_s}$, circumferential, $\overline{\tau}_{w_z}$, spanwise. The wall-shear stresses are normalized by an upstream $\overline{\tau}_{w_s}$ at s=-4 ($\overline{\tau}_{w_s,in}$).

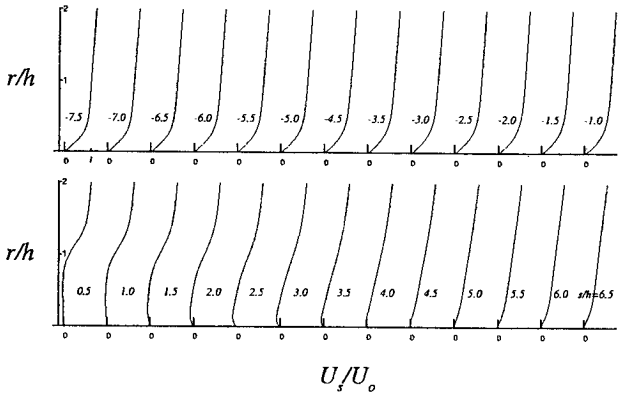

Fig. 4 Profiles of the mean circumferential velocity component (U_s) at selected s locations. Here, r denotes the radial coordinate measured in the direction locally normal to the cylinder surface.

of grid spacing in wall units. The averaged spanwise wall-shear stress is nearly zero along the cylinder surface as it should be since the flow is homogeneous in the spanwise direction. This also confirms that the duration of averaging was adequate.

In Fig. 4, the profiles of the mean circumferential velocity component (U_s) are shown at selected s locations; each profile represents the radial distribution of U_s normalized by U_o. The main recirculating region is clearly seen, even though the shape of each profile is quite different from those in plane backward-facing step flow. See Fig. 17 of Le *et al.*[7] With respect to the rotating reference frame, U_s is linearly increasing in the radial direction as r goes to infinity. One can also notice that the flow past the step is quickly re-established and approaches the next step with constant $\overline{\tau}_{w_s}$. See the region for $-5 \leq s \leq -3$. The secondary recirculating region is much smaller than the counterpart in the plane backward-facing step flow. See the profile at s/h=0.5 and Fig. 2 of this paper and Fig. 8 and the profile at x/h=0.5 in Fig. 17 of Le *et al.*[7]

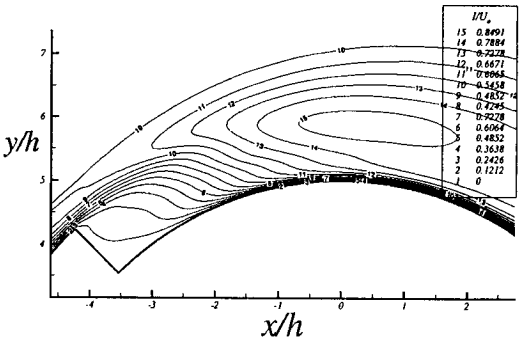

Fig. 5 Distribution of the mean turbulence intensity near the step, normalized by U_o.

Turbulence intensity and wall-shear stress fluctuation

Figure 5 shows the mean turbulence intensity ($I = \sqrt{\overline{u_i'u_i'}/3}$ where u_i' is the velocity fluctuation in each direction) around the step, normalized by U_o. Steep normal variation of I is noticed along a wide range of the cylinder surface. Furthermore, the maximum I is observed one h away from the cylinder surface above the reattachment point. This is consistent with the observation of Nesic *et al.*[3] They claimed that the most important factor for mass-transfer-controlled erosion-corrosion in turbulent flows is not $\overline{\tau}_{w_s}$ but local I near the cylinder surface, and that severe corrosion is observed near the reattachment point in suddenly-expanded pipe flows, where high turbulent fluctuation

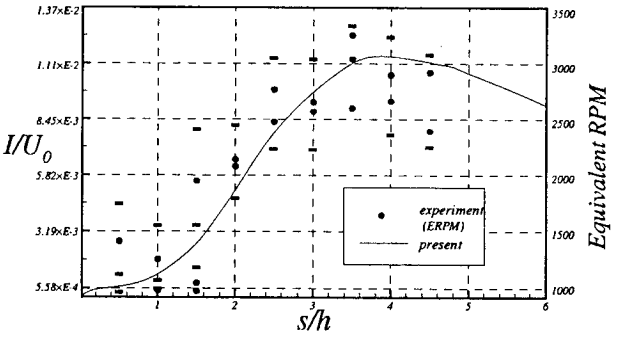

Fig. 6 Distribution of the mean turbulence intensity along the cylinder surface, computed at 0.006h away from the surface, together with the hot film measurements[5] at 2,000rpm indicating the mass-transfer capacity.

is normally observed.

In Fig. 6, distribution of I along the cylinder surface, computed at 0.006h away from the surface, is shown together with the hot film measurements[5] indicating the mass-transfer capacity. Here, 'Equivalent RPM'(ERPM) represents normalized values using

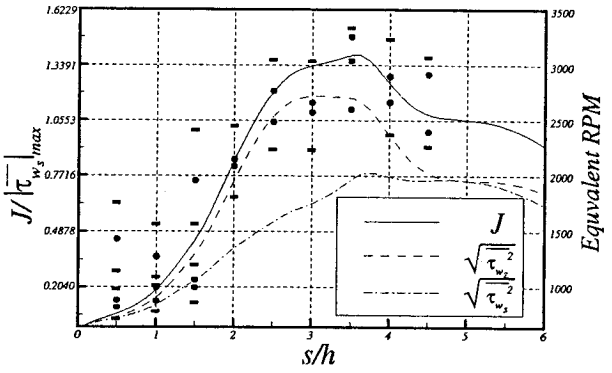

Fig. 7 Distribution of the rms of wall-shear stress fluctuation along with the mass-transfer capacity.[5]

those of the circular cylinder without the steps; a value larger (less) than 2,000ERPM means higher (lower) mass-transfer capacity than the no-step counterpart.[4] The range between two small rectangles at a given s indicates an error bar, and the small circles represent typical measurements at that s. Since I and ERPM have different dimensions, quantitative comparison cannot be made between the two. Nevertheless, qualitative comparison can be made regarding the tendency of mass-transfer capacity along the cylinder surface and the location of the maximum value. Figure 6 reveals that the computation predicts a wide range of high mass-transfer capacity ($3.5 \leq s \leq 4.5$) which is consistent with the experimental measurement; in this range of s, the mean turbulence intensity also has a steep normal gradient(Fig. 5).

Fluctuation of wall-shear stress is another factor which plays an important role in mass-transfer-controlled erosion-corrosion. In Fig. 7, is shown the distribution of the computed root-mean-square(rms) of wall-shear stress fluctuation ($J = \sqrt{\overline{\tau_w'^2}}$) along the cylinder surface. Here, both the circumferential and the spanwise components are considered and plotted, i.e.

$$J = \sqrt{\overline{\tau_w'^2}} = \sqrt{\overline{\tau_{w_s}'^2 + \tau_{w_z}'^2}}. \qquad (4)$$

Figure 7 also shows the distribution of the mass-transfer capacity[5] using hot film measurements. The computed data of J well (even better) match the experimental results; this suggests that not only turbulence intensity but also wall-shear stress fluctuation can significantly affect the mass-transfer-controlled erosion-corrosion. Other Interesting features include that the rms of the wall-shear stress fluctuation is of the same order or larger than the mean value (Fig. 3) throughout the domain, and that the spanwise component ($\sqrt{\overline{\tau_{w_z}'^2}}$) is dominant in the range of maximum J. The latter will be given more detailed explanation in the next section.

Instantaneous velocity and vortical fields

To illustrate large-scale unsteadiness and three-dimensionality in the turbulent flow, Fig. 8 shows the regions of instantaneous reversed flow at two different spanwise locations but at the same time (Fig. 8(a) and 8(b)), and at two different times approximately 2.7 revolutions apart but at the same spanwise location (Fig. 8(a) and 8(c)). The flow structures are quite different both in space and in time as one can expect in turbulent flows. The location of the instantaneous reattachment point of the main recirculating region varies considerably up to approximately $3h$ in time and space as in a plane backward-facing step flow.[7] This explains why the hot-film measurement at the same rpm (Fig. 6 or 7) has a not distinct but relatively smeared peak.

The instantaneous reattachment points on a typical spanwise (x-y) plane are depicted during three revolutions of the cylinder in Fig. 9; the symbols represent the reattachment points measured by zero τ_{w_s}. It is seen that the recirculating region periodically stretches out on the cylinder surface; simultaneously it breaks into pieces (e.g. $1.0 \leq t/T \leq 1.2$, where T is the period of the cylinder rotation). Figure 8(b) clearly shows this situation. The same trend was observed in the plane backward-facing step flow; see Fig. 3 of Le *et al.*[7] They pointed out that as the large-scale structure created by the shear-layer roll-up grows, the reattachment location travels downstream at a constant speed. They also noted that the sudden decrease of the reattachment length indicates a detachment of the turbulent large-scale structure from the step. All these observations also hold in the current case.

Figure 10 exhibits magnitude contours of normalized instantaneous fluctuation of the wall-shear stress ($\sqrt{\tau_{w_s}'^2 + \tau_{w_z}'^2}/|\overline{\tau}_{w_s}|_{max}$) on the cylinder surface downstream of the step; Figs. 10(a) and 10(b) are corresponding to Figs. 8(a) and 8(c), respectively in time. It can be noticed that the wall-shear stress significantly varies between s/h=2.0 and s/h=5.0, consistent with the peak range in Fig. 6 or 7. Furthermore, one can estimate that the maximum magnitude of the instantaneous wall-shear stress fluctuation is three or four times larger than the maximum mean value (Fig. 3). Such intense wall-shear stresses occur locally and intermittently.

Recalling that the mean spanwise wall-shear stress ($\overline{\tau}_{w_z}$) is nearly zero all along the cylinder surface (Fig. 3), the high spanwise wall-shear stress fluctuation (Fig. 7) implies the presence of strong streamwise vortices. In Fig. 11, are shown contours of instantaneous streamwise vorticity (ω_s) on the plane perpendicular to the cylinder surface at s/h=3.5 at two different times; solid and dashed lines represent positive and negative values, respectively. Pairs of strong ω_s are clearly identified at any instant; similar streamwise

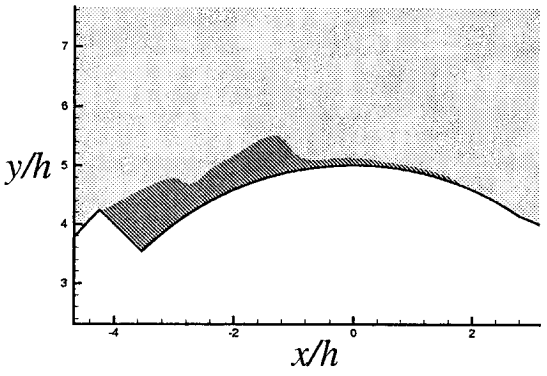

a) $z = z_1, t = t_1$

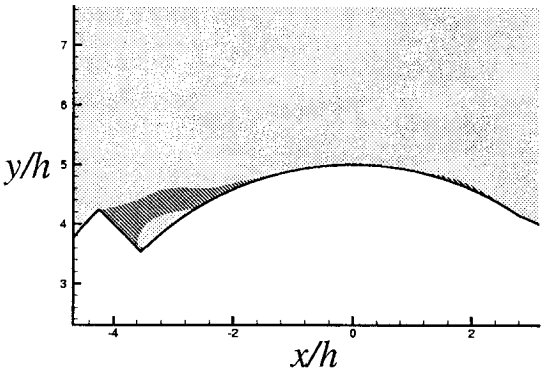

b) $z = z_1 + W/2, t = t_1$

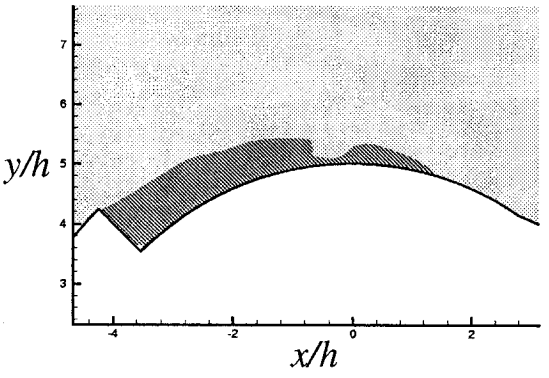

c) $z = z_1, t = t_1 + 2.7T$

Fig. 8 Regions of instantaneous reversed flow, where T is the period of the cylinder rotation.

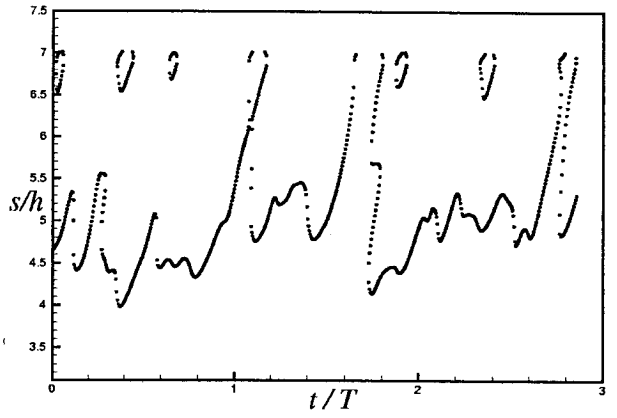

Fig. 9 Instantaneous reattachment points on a typical spanwise (x-y) plane.

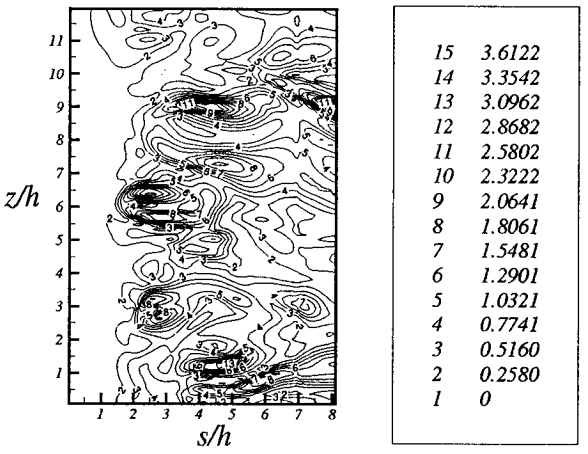

a) $t = t_1$

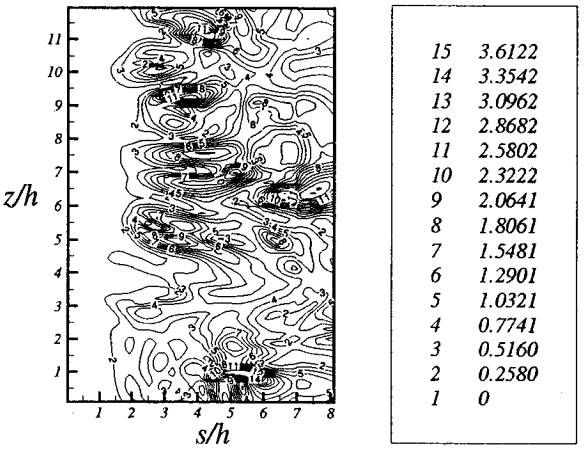

b) $t = t_1 + 2.7T$

Fig. 10 Magnitude contours of normalized instantaneous fluctuation of the wall-shear stress ($\sqrt{\tau'_{w_s}{}^2 + \tau'_{w_z}{}^2}/|\overline{\tau}_{w_s}|_{max}$) on the cylinder surface downstream of the step.

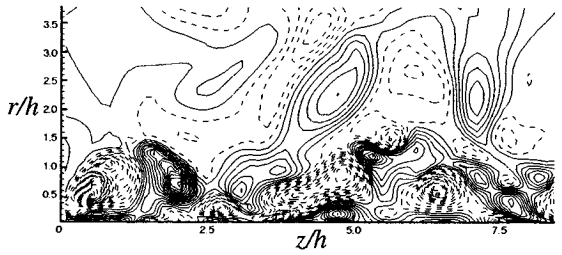

a) $t = t_1$

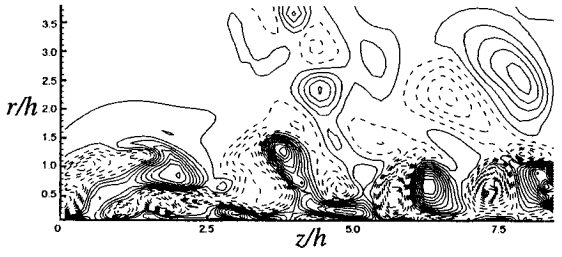

b) $t = t_1 + 3.1T$

Fig. 11 Contours of instantaneous streamwise vorticity (ω_s) at s/h=3.5, normalized by U_o/h, $\Delta\omega_s h/U_o$=0.19.

vortices were observed in the plane backward-facing step flow. See Fig. 6 of Le *et al.*[7]

Conclusion

In this investigation, turbulent flow around a rotating cylinder with backward-facing steps mounted symmetrically with respect to the axis of rotation was numerically studied using DNS. The results are presented with respect to the rotating reference frame in which the cylinder is stationary and the outer boundary is ratating. A rotational speed of 2,000rpm in the air is considered. A main recirculating region is formed downstream of the step. Although the basic flow field is completely different from that of a plane backward-facing step flow, the structures and unsteady characteristics of the main recirculating region have many features in common with those of a plane backward-facing step flow.

Intense turbulent fluctuation and its steep normal gradient are observed in the vicinity of the cylinder surface in the recirculating region, especially near the reattachment point. Strong wall-shear stress fluctuation is also detected along the cylinder surface in a wide range of 2 to 5 step heights downstream of the step. This is consistent with the range of high mass-transfer capacity experimentally observed. Since erosion-corrosion is mass-transfer controlled, it is confirmed that turbulence effects, such as turbulent fluctuation and wall-shear stress fluctuation, can accelerate the rate of erosion-corrosion. The results obtained also reveal the practical applicability of the rotating cylinder as a economic and tractable tool for corrosion research.

Acknowledgment

This research was financially supported by Korea Science and Engineering Foundation(98–0200–12–01–3). The computing cost was partially covered by the University of Queensland.

References

[1]J. Postlethwaite, M. H. Dobbin, and K. Bergevin, "The role of oxygen mass transfer in the erosion-corrosion of slurry pipelines", *Corrosion*, Vol. 42, 1986, pp. 514-521.

[2]B. K. Mahato, S. K. Voora, and L. W. Shemilt, "Steel pipe corrosion under flow conditions - I. An isothermal correlation for a mass transfer model", *Corros. Sci.*, Vol. 8, 1968, pp. 173-193.

[3]S. Nesic, and J. Postlethwaite, "Relationship between the structure of disturbed flow and erosion-corrosion", *Corrosion*, Vol. 46, No. 11, 1990, pp. 874-880.

[4]D. C. Silverman, "Rotating cylinder electrode-geometry relationships for prediction of velocity-sensitive corrosion", *Corrosion-NACE*, Vol. 44, No. 1, 1988, pp. 42-49.

[5]S. Nesic, J. Bienkowsky, K. Bremhorst, and K.-S. Yang, "A compact apparatus for testing erosion-corrosion under disturbed flow conditions consisting of a rotating cylinder with a step", *Corrosion*, Vol. 56, No. 10, 2000, pp. 1005.

[6]B. F. Armaly, F. Durst, J. C. F. Pereira, and B. Schönung, "Experimental and theoretical investigation of backward-facing step", *J. Fluid Mech.*, Vol. 127, 1983, pp. 473–496.

[7]H. Le, P. Moin, and J. Kim, "Direct numerical simulation of turbulent flow over a backward-facing step", *J. Fluid Mech.*, Vol. 330, 1997, pp. 349-374.

[8]D. K. Lezius, and J. P. Johnston, "Roll-cell instabilities in rotating laminar and turbulent channel flows", *J. Fluid Mech.*, Vol. 77, 1976, pp. 153–175.

[9]E. W. Adams, J. P. Johnston, and J. K. Eaton, "Experiments on the structure of turbulent reattaching flow", Rep. MD-43, Thermosciences Division, Dept. of Mech. Engng., Stanford University, 1984.

[10]M. Rosenfeld, D. Kwak, and M. Vinokur, "A Fractional Step Solution Method for the Unsteady Incompressible Navier-Stokes Equations in Generalized Coordinate Systems", *Journal of Computational Physics*, Vol. 94, 1994, pp. 102-137.